# Influence of solution rate and substrate temperature on the properties of lead iodide films deposited by spray pyrolysis

**J. F. Condeles · M. Mulato**

**Abstract** Polycrystalline lead iodide (PbI$_2$) thin films have been deposited by spray pyrolysis method using *N,N*-dimethylformamide (DMF) as solvent as a function of several deposition parameters. DMF is used as an alternative to water due to the larger solubility limit of PbI$_2$ in this solvent. In this work, the solution rate during the deposition time of 3 h was varied in the range of 0.11 cm$^3$/min up to 0.30 cm$^3$/min. A growth rate varying from 19 Å s$^{-1}$ up to 47 Å s$^{-1}$ was obtained as a function of solution rate. Dark current as a function of temperature for the final films reveals that for larger solution rates smaller values of electrical resistivity is obtained. For a solution rate of 0.30 cm$^3$/min, an electrical transport activation energy ($E_a$) of about 0.65 eV was measured for the whole temperature range. On the other hand, for the sample deposited with a solution rate of 0.11 cm$^3$/min, two main transport mechanisms can be observed with an activation energy of about 1.23 eV for temperatures above 50 °C. The effect of substrate temperature is also discussed. Samples were deposited in the temperature range of 170 °C up to 250 °C with a fixed solution rate of 0.16 cm$^3$/min. In addition, the films were exposed to X-ray irradiation in the mammography diagnosis region, using a molybdenum (Mo) anode and a peak tube potential between 26 and 36 kV (equivalent photon energies between 10 keV and 15 keV).

J. F. Condeles
Universidade Federal do Triângulo Mineiro (UFTM),
Av. Frei Paulino 30, Uberaba, MG 38025-180, Brazil

M. Mulato (✉)
Departamento de Física e Matemática, Faculdade de Filosofia, Ciências e Letras de Ribeirão Preto, Universidade de São Paulo, Av. Bandeirantes 3900, Ribeirão Preto, SP 14040-901, Brazil
e-mail: mmulato@ffclrp.usp.br

## Introduction

In the last few years, great interest has been focused on high atomic number and wide band-gap semiconductor materials for applications in room temperature ionizing radiation detection. Some compound semiconductor materials such as PbI$_2$, HgI$_2$, TlBr, CdTe, and CdZnTe are good photoconductors that can be used at room temperature [1–3]. These materials when deposited in film form have been suitable as promising semiconductor candidates for applications in ionizing radiation detectors, with a technological applicability on the development of the active matrix flat panel imagers (AMFPIs) for medical applications in digital radiography [1, 4]. There are two types of AMFPIs which may be defined as: (i) indirect detection method, the scintillating layer (phosphor for example) converts X-ray photons into optical photons (i.e. with wavelength in the visible range), which in turn are absorbed by the p-i-n a-Si:H photodetector [1, 5] and (ii) direct detection method, X-rays interact with a semiconductor layer, where they are directly converted into electric charge and the electric signal response is proportional to the amount of exposure on each pixel. An external electric field is applied across the photoconductor allowing the collection of charge in each pixel [1, 3, 6]. For the same quality of the final image, the direct detection method is better since a lower dose would be administered to the patient. The dose for a mammogram is high because of the low photon energies used to maximize soft tissue image contrast [7]. In this sense, a lower dose would be used to obtain the same quality of the final image using the direct detection method.

As a good candidate, lead iodide presents a wide band-gap (above 2.0 eV) [8], high stopping power for ionizing radiation due to its high atomic number (i.e., *Z* = 82 for Pb

and $Z = 53$ for I) and high mass density (6.2 g/cm$^3$) [9]. Several methods have been used to fabricate lead iodide films such as physical vapor deposition (PVD) [10–12], solution growth [13], spray pyrolysis [14], and vacuum evaporation [6]. The main physical properties of PbI$_2$ as single crystal (bulk) are already well known and have been reported by several researchers that obtained samples with good crystalline properties [15–17]. Therefore, there are few papers related to the study of polycrystalline PbI$_2$ deposited in the form of films, which is the most useful for medical imagers for instance [2]. In our case, spray pyrolysis has been used as an alternative deposition method for the fabrication of polycrystalline PbI$_2$ films using $N,N$-dimethyl-formamide (DMF) as an organic solvent for dissolution of the PbI$_2$ [18]. Spray pyrolysis is used because it has a relative slow cost and it also allows the fabrication of films on top of large areas. DMF is used because larger amounts of PbI$_2$ are dissolved in this solvent when compared to water. The optical and structural properties of PbI$_2$ films deposited by spray pyrolysis using DMF as solvent were also already previously reported [18]. Thus, in this work we present a comprehensive study of the effects of two other main deposition parameters, respectively, the solution rate and the substrate deposition temperature on the morphology and electrical properties of the final films. The electrical properties are investigated in the dark and under illumination using irradiation in the mammography energy region.

## Materials and methods

The spray pyrolysis deposition method was already previously described [14]. A home-made apparatus has been designed and assembled to overcome limitations of previous systems such as reproducibility, temperature control, and spray-nozzle to substrate distance. The lead iodide films were deposited from highly pure starting powder (99.999%), produced and commercially available by Aldrich Co. The powder was dissolved in $N,N$-dimethyl-formamide (DMF) organic solvent at room temperature for solution preparation. A solution concentration of 40 g/L was used. The films were deposited on Corning 7059 glass substrates during 3 h, the distance between the spray-nozzle to substrate was kept constant at 20 cm and the nitrogen atmosphere into the chamber was operated at a flow rate of $8.0 \times 10^3$ cm$^3$ min$^{-1}$. For the first experiment, samples were produced using varied solution rates in the range of 0.11 cm$^3$/min up to 0.30 cm$^3$/min, for a fixed substrate temperature of 250 °C. For the second experiment, the films were deposited in the substrate temperature range from 175 to 250 °C, with the solution rate kept constant at 0.16 cm$^3$/min. The morphology of the samples was investigated by scanning electron microscopy (SEM).

The samples were also electrically characterized in the dark and under X-ray irradiation in the energy region of mammography diagnosis.

For electrical characterizations in the dark and under X-ray exposure, the detectors were assembled using palladium (Pd) contacts in the coplanar configuration, which were previously evaporated on the surface of the substrates. Pd was chosen because it makes ohmic contact with PbI$_2$ [19]. The dark current was recorded as a function of temperature in the range from $-10$ °C to 110 °C using a Hewlett Packard pA meter/dc voltage source (4140B). The measurements were performed with the temperature raised at a constant rate of 3 °C/min, while the sample was kept in vacuum. A Tektronix programmable power supply (P2511G) was used for temperature increase by Joule effect, while liquid nitrogen was used to cool down the sample. The photocurrent as a function of exposure in the range of mammography diagnosis was measured using a General Electric Senographe 500T mammography X-ray source with a molybdenum (Mo) anode (k$_\alpha$ radiation of 17.5 keV) with 0.5 mm Al filtration. This equipment can provide pulses with exposure times from 0.6 s up to 2.3 s. Exposure was measured with a Radcal dosimeter (model 9015) using a Radcal Corporation ionization chamber (model 10X5-6) and the electrical signal was recorded on a Keithley electrometer (model 610 C). X-ray tube potentials of 26 kVp and 36 kVp resulting in equivalent photon energies of 10 keV and 15 keV were used. The distance between X-ray source and the samples was 45 cm. An electric field of 125 V/cm was applied to the sample.

## Results and discussions

Figure 1 presents the average growth rate as a function of solution rate in the range of 0.11 cm$^3$/min up to 0.30 cm$^3$/min. The samples were fabricated at 250 °C during 3.0 h using a solution concentration of 40 g/L. The thicknesses of the samples were calculated using cross-section SEM pictures. An average growth rate varying from 19 Å s$^{-1}$ up to 47 Å s$^{-1}$ was obtained as a function of solution rate. The average growth rate increases linearly with the solution rates used in each deposition. This result indicates that for the spray pyrolysis technique there is direct proportionality between the growth rate and the amount of material that is dropped on top of the substrates. We do not observe a final thickness limitation as already reported in the literature [11].

The surface of the samples was investigated by scanning electron microscopy, and the results for the two extreme solution rates of 0.11 cm$^3$/min and 0.30 cm$^3$/min are presented in Fig. 2. Figure 2a, b corresponds to the smaller rate, while Fig. 2c, d corresponds to the larger rate. It can be clearly seen that the larger solution rate leads to a more
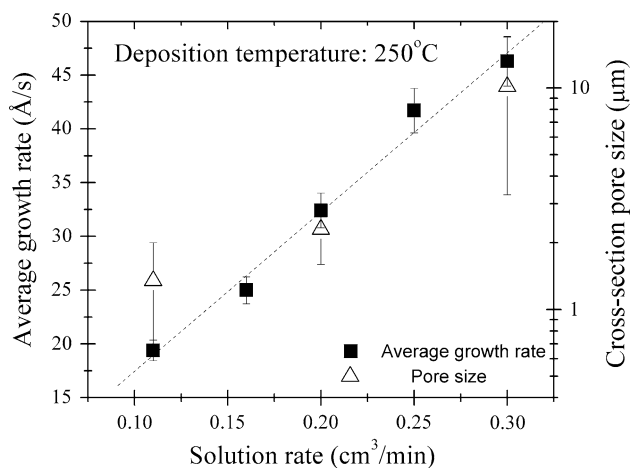
**Fig. 1** *Left* linear dependence of the average growth rate (*filled square*) and *right* non-linear dependence of pore size as determined by the average diameter using cross-section SEM images (*open triangle*). Data presented as a function of solution rate. Total deposition time of 3.0 h at a substrate temperature of 250 °C, using a concentration of 40 g/L (PbI$_2$ in DMF)

porous material. The amount of surface defects seem to be smaller for the sample deposited at lower solution rate because of better surface coverage. We believe that the growth mechanism changes as a function of solution rate due to the variation of the amount of droplets that arrive on top of the substrates as a function of time. With increasing growth rates the process is somehow more aggressive, probably because a larger amount of solvent has to evaporate during the same time interval, leading to the fabrication of the observed pores. The pore size as determined by the average diameter using cross-section SEM images

are presented as triangles in Fig. 1. Note the logarithmic scale at the right y-axis of the figure.

In addition, as visually observed, the size of the droplets leaving the nozzle-spray increases with increasing solution rate, for a fixed nitrogen flow. Some papers have already addressed the behavior of the droplets during transport and evaporation at the substrate [20–22]. It was proposed that the droplets experience evaporation leading to size reduction and the creation of a concentration gradient within the droplet. For a situation where the solubility limit is reached the solute precipitates on the surface. This might happen due to the slow solute diffusion. When in contact with the heated substrate the situation is even more pronounced, with much more solute material concentration at the bottommost part of the droplet. The internal excess solvent material would leave the surface of the droplet causing an explosion and leading to the observed craters-like structures. An ideal deposition condition is when a small number of droplets with small sizes approach the substrate. Deviations from the ideal condition occur when the droplet size and their amount on top of the substrate vary as a function of increasing solution rate. Higher solution rates lead to larger droplets increasing the porosity because of the smaller ad-atoms mobility on the surface of the substrate and faster evaporation of a larger amount of solvent.

The final structure and morphology of the surface of the samples are very important for electronic applications. The carrier's mobility is associated also with imperfect contacts between grain boundaries, and also between grains and metal electrodes. The problem seems to be smaller for the samples deposited at lower solution rates because of better surface coverage.

**Fig. 2** SEM pictures of the surface of the samples fabricated under similar conditions as in Fig. 1. **a** and **b** solution rate of 0.11 cm$^3$/min, and **c** and **d** solution rate of 0.30 cm$^3$/min
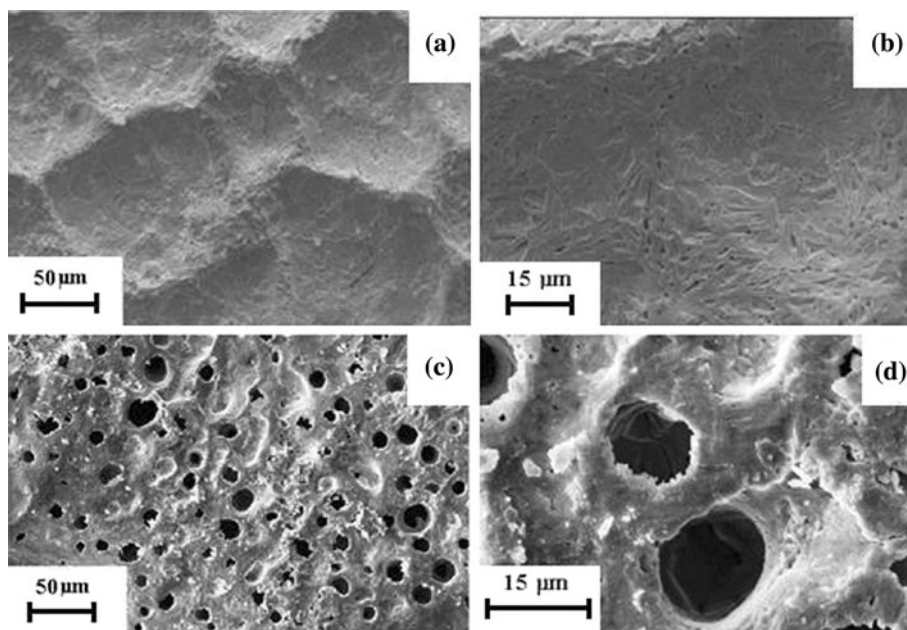
The electrical resistivity was obtained in the dark at room temperature for all the samples deposited at different solution rates. The variation of electrical resistivity as a function of average growth rate is presented in Fig. 3. A non-linear dependence was observed, and the maximum value was obtained for the smallest deposition rate of about 19 Å $s^{-1}$. For larger growth rates a drastic decrease is observed and a possible saturation might even occur. We believe that this is determined by the fabrication process: when the solution hits the substrate and evaporates it leads to a film with varying structural defects. As already discussed, the larger the deposition rate, the larger the amount of pores and defects, which in this case contributes for a decrease in electrical resistivity. The more aggressive the evaporation process, the larger the amount of defects, and the smaller the electrical resistivity. Similar results have been published for $MnO_2$ films also deposited by spray pyrolysis [23]. The authors reported a linear dependence of growth rate with solution rate for values up to 0.8 $cm^3$/min. As a consequence, the electrical resistivity of $MnO_2$ also decreases as a function of growth rate. Thus the result seems to be intrinsic to the fabrication technique. For the case of our lead iodide films, the largest value of electrical resistivity was about $1 \times 10^{10}$ Ωcm, as seen in Fig. 3. On the other hand, for films fabricated using other techniques this value was previously reported as: (i) $6 \times 10^{11}$ Ωcm for films fabricated using solution growth [13], (ii) $8 \times 10^{12}$ Ωcm for films fabricated by sublimation of purified starting powder, during 10 days at a rate of 10 μm/day [24]; (iii) $3 \times 10^{10}$ Ωcm [25] and $10^{12}$ Ωcm [6] for vacuum evaporated films. Note that these values are always smaller than the one reported for the bulk, which is of the

order of $10^{13}$ Ωcm [17, 26, 27]. Lead iodide crystals in the bulk form can also be intentionally doped leading to a variation of resistivity values down to $10^7$ Ωcm [28]. This shows that the lead iodide films, regardless of the fabrication technique, might have a larger amount of defects or even non-intentional doping than the bulk. This is a point that needs to be optimized for future applications of the material in medical imaging.

A deeper investigation of the electrical properties of the samples was done by measuring the dark current as a function of temperature. The results in Fig. 4 correspond to two samples fabricated using solution rates of 0.11 and 0.30 $cm^3$/min, respectively, and for a fixed deposition temperature of 250 °C. An external electrical field of 125 V/cm was used. For the sample deposited using a solution rate of 0.30 $cm^3$/min, an activation energy ($E_a$) of about 0.65 eV was measured for the whole temperature range. This indicates that a single transport mechanism dominates the transport of carriers, with low energy transition into the band-gap. The fact that $E_a$ is smaller than half the band-gap of the material, which is 2.4 eV [19], reveals that there are deep levels into the band-gap and these levels are probably due to either intrinsic defects of the sample such as dangling bonds from the grain boundaries and/or distorted bonds or non-intentional doping. On the other hand, for the sample deposited with a solution rate of 0.11 $cm^3$/min, the results indicate the presence of two transport mechanisms. The data presented in Fig. 4 (as circles) satisfy the thermally activated dark current relation
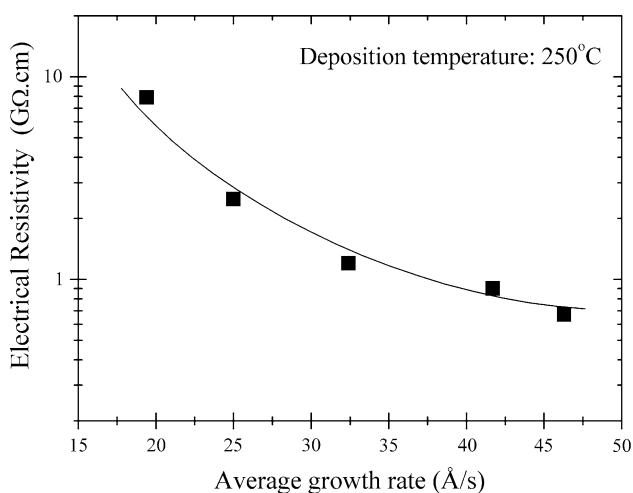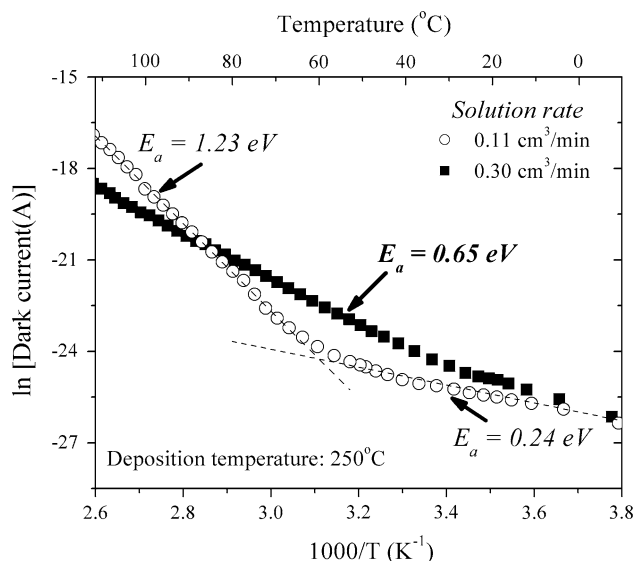


**Fig. 3** Electrical resistivity in the dark, as a function of average growth rate for samples deposited adopting a total deposition time of 3.0 h at a substrate temperature of 250 °C, and using a concentration of 40 g/L ($PbI_2$ in DMF)



**Fig. 4** Dark current as a function of inverse temperature for the same two samples of Fig. 2, i.e., *open circles* represent a solution rate of 0.11 $cm^3$/min and *solid squares* represent a solution rate of 0.30 $cm^3$/min. An electric field of 125 V/cm was applied for using co-planar configuration. The calculated activation energies are indicated

$$I_{dc} = I_1 \exp\left(\frac{-E_1}{K_B T}\right) + I_2 \exp\left(\frac{-E_2}{K_B T}\right) \qquad (1)$$

where $K_B$ is the Boltzmann's constant, and $T$ is the temperature. For temperatures above 50 °C (first left region) a value of 1.23 eV was obtained. The conduction mechanism is due to band-to-band transitions. For temperatures below 50 °C (second right region) the activation energy is 0.24 eV. The conduction mechanism is due to hopping in the localized defect states (dangling bonds). The fact that an activation energy of 1.23 eV was obtained for this sample indicates the importance of defects in respect to non-intentional doping. This is in agreement with the previously discussed structural and morphological data. Previously reported values of $E_a$ were: (i) 0.1 e V for intentionally doped samples [13]; (ii) 0.3 eV for temperatures below 180 °C and 1.7 eV for temperatures above 200 °C, for non-doped single crystals [19]; (iii) 0.78 eV for vacuum evaporated films [25]; and (iv) 0.43 eV for films deposited at 225 °C obtained by spray pyrolysis using water-dissolved $PbI_2$ as a solvent [14]. In this sense the values of the films of the present work are quite reasonable, and they confirm that the smaller the solution rate the better the electrical properties of the final sample.

The studies of the influence of solution rate and deposition temperature on the electrical properties of the films were carried out in parallel. Films were deposited in the temperature range from 175 °C up to 250 °C, with a constant solution rate of 0.16 cm³/min. The surface of the samples as a function of deposition temperature was investigated by SEM in a previous contribution [18]. It was shown that increasing deposition temperatures leads to lower porosity. In the present contribution, the dark current as a function of temperature was investigated for all considered deposition temperatures. Figure 5 shows the experimental results and the fitted regions for the extraction of the $E_a$ values. For the sample deposited at the smallest substrate temperature of 175 °C, an activation energy of about 0.45 eV was obtained for the whole temperature range. A single transport mechanism dominates, and the low value of $E_a$ indicates a large contribution of sub band-gap defects. For the other samples deposited above this temperature (i.e. from 200 °C up to 250 °C) two main transport mechanisms can be observed. For the low temperature region bellow 30 °C, the activation energy varies as a function deposition temperature from 0.39 eV down to 0.31 eV with increasing fabrication temperature. For temperatures above 45 °C the activation energy increases as a function of deposition temperature from 0.62 eV up to 1.13 eV.

Figure 6a shows the values of activation energy as a function of deposition temperature. Note that $E_1$ increases in an exponential way, while the decrease of $E_2$ with
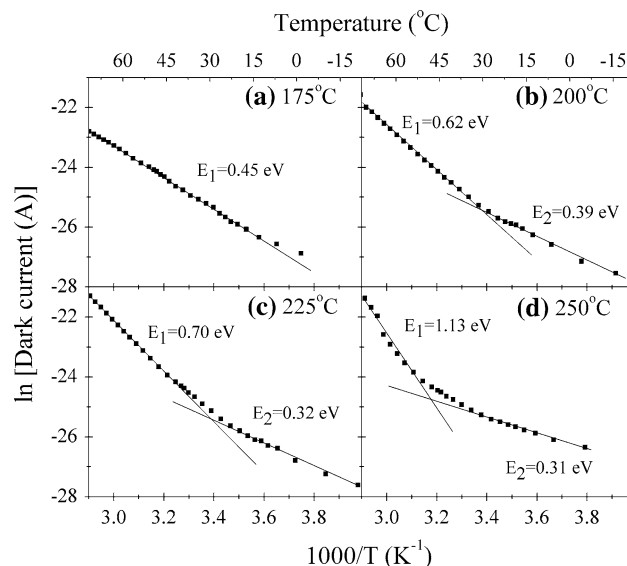


**Fig. 5** Dark current as a function of inverse temperature for the samples deposited at **a** 175 °C, **b** 200 °C, **c** 225 °C, and **d** 250 °C. The solution rate was kept constant at 0.16 cm³/min and an electric field of 125 V/cm was used in the co-planar configuration. The activation energies for processes that dominate the transport for high and low temperatures are named $E_1$ and $E_2$, respectively

deposition temperature is quadratic only. For a deposition temperature of 250 °C, $E_1$ reaches half the optical band-gap as desired, but deep defects still exist and can be observed at low temperatures. We believe that other fabrication parameters should be optimized to reduce this contribution. Increasing the deposition temperature to higher levels might not be capable to solve the problem alone. Figure 6b shows the values of inverse temperature where the transition between the two transport mechanisms is observed. Note that the higher the deposition temperature, the larger the transition temperature. This indicates that the desired transport mechanism with larger activation energy dominates the response of the samples for a smaller temperature range. We believe that for the low temperature region, localized hopping and/or transitions due to donor and acceptor levels of impurities might be the dominating mechanism, while for the temperature region above 45 °C band-to-band transitions seem to be the main contribution. The higher the fabrication temperature, the better the electrical properties of the films with an activation energy that can even reach half the optical band-gap as desired. Nevertheless, undesired electronic states close to the conduction and valance bands still exist and must be eliminated by the optimization of other deposition parameters or post-fabrication treatments. Table 1 presents the comparison of the activation energies for the samples of the present investigation with others reported in the literature.

The sample that presented the largest activation energy was submitted to X-ray exposures in the range of
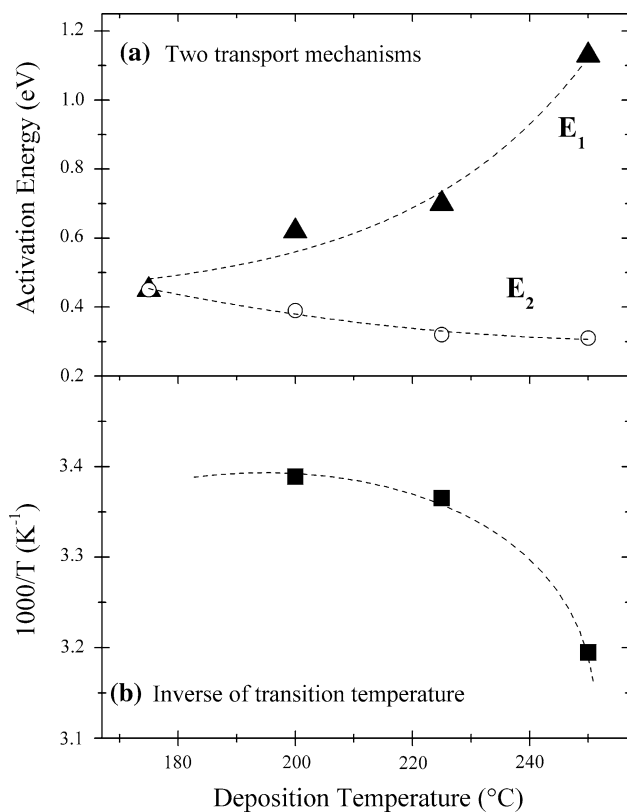
Fig. 6 a Activation energies $E_1$ (*top curve*) and $E_2$ (*bottom curve*) corresponding to different transport mechanisms, as obtained from Fig. 5, as a function of substrate deposition temperature. The upper curve is an exponential fitting, while the bottom curve is a second order polynomial fitting. b Inverse of transition temperature where the separation between the two transport mechanisms occur. The *dashed line* is a guide for the eyes
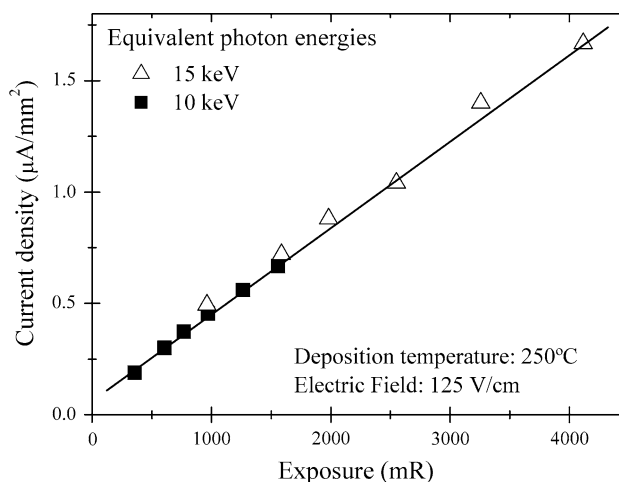


Fig. 7 X-ray photocurrent density as a function of exposure, for varying photon energies in the range of mammographic diagnosis. An electric field of 125 V/cm was used, and the sample was fabricated at 250 °C, using a solution rate of 0.16 cm³/min

mammographic diagnosis, as presented in Fig. 7. The current density as a function of exposure was recorded from 360 mR up to 4100 mR, using two values of equivalent photon energies, as indicated. Note that there is no energy selection, and that the response is very linear with a slope of 40 $\mu$A/cm$^2$ R. One of the most important properties of a detector is high sensitivity for minimum dose. In this sense, the larger the response of the sensor, the

better its chance for usage in technological applications. Compared to previously reported detectors, the answer of the present $PbI_2$ samples is 2.5 times better than for $HgI_2$ [1], and it is about 7 times better than for $PbI_2$ [1]. This illustrates the potential application of the technique and the material for future use in medical imaging.

## Conclusions

We have investigated the fabrication of lead iodide films by using spray pyrolysis with DMF as precursor solvent. The influence of solution rate and deposition temperature on the final properties of the samples was investigated. The variation of the solution rate leads to a linear variation of the growth rate, but leads to a final morphology with increasing porosity. The effect is also seen in the reduction of the electrical resistivity with increasing solution rate, what seems to be intrinsic to the fabrication technique. The smaller resistivity is due to the deep defects inside the

**Table 1** Comparison of activation energy values according to the fabrication technique

| Fabrication method | Activation energy $E_a$ (eV) | Reference number |
|---|---|---|
| Solution growth, intentionally doped | 0.1 | [13] |
| Single crystals grown in gels $T < 180$ °C | 0.3 | [19] |
| Spray pyrolysis using water as solvent, $T = 225$ °C | 0.43 | [14] |
| Spray pyrolysis using DMF as solvent, $T = 175$ °C | 0.45 | This work |
| Spray pyrolysis using DMF as solvent, $T = 200$ °C | 0.62/0.39 | This work |
| Spray pyrolysis using DMF as solvent, $T = 225$ °C | 0.70/0.32 | This work |
| Vacuum evaporated films | 0.78 | [25] |
| Spray pyrolysis using DMF as solvent, $T = 250$ °C | 1.13/0.31 | This work |
| Single crystals grown in gels $T > 200$ °C | 1.7 | [19] |

From left to right, fabrication method, activation energy and reference

band-gap of the material, which contribute also to a reduction of the activation energy. Using small solution rates, an activation energy close to half the optical band-gap can be reached, as desired. Nevertheless, the sub band-gap mechanisms are not totally eliminated. Increasing deposition temperatures up to 250 °C leads to activation energy variation from 0.45 up to 1.13 eV. The mechanism due to the higher activation energy is strongly dependent on deposition temperature, but the temperature value where transition occurs is displaced toward larger temperature values. This indicates that the transport due to localized hopping is not totally eliminated, besides the strong reduction of states in the central part of the band-gap. The values of activation energy here reported sits in the upper limit for the specific temperature range up to now. Some other deposition parameters could also influence the structure and the transport properties of the material and should be investigated in the future. The sample with larger activation energy was tested under mammography diagnosis energy range, showing a linear response. We believe that the material could be an interesting candidate for the development of X-ray detectors for digital radiography imaging using the direct detection technique. For that aim, further optimizations are required.

## References

1. Street RA, Ready SE, Schuylenbergh KV, Ho J, Boyce JB, Nylen P, Shah K, Melekhov L, Hermon H (2002) J Appl Phys 91:3345
2. Condeles JF, Ghilardi Netto T, Mulato M (2007) Nucl Instrum Methods A 577:724
3. Kasap SO, Rowlands JA (2002) IEE Proc Circuits Devices Syst 149(2):85
4. Bennett PR, Shah KS, Dmitriev Y, Klugerman M, Gupta T, Squillante M, Street R, Partain L, Zentai G, Pavyluchova R (2003) Nucl Instrum Methods A 505:269
5. Lemmi F, Mulato M, Ho J, Lao R, Lu JP, Street RA, Palma F (2001) Appl Phys Lett 78(10):1334
6. Shah KS, Street RA, Dmitriyev Y, Bennett P, Cirignano L, Klugerman M, Squillante MR, Entine G (2001) Nucl Instrum Methods A 458:140
7. Condeles JF, Lofrano RCZ, Rosolen JM, Mulato M (2006) Braz J Phys 36(2A):320
8. Ahuja R, Arwin H, Ferreira da Silva A, Persson C, Osório-Guillén JM, Souza de Almeida J, Moyses Araujo C, Veje E, Veissid N, An CY, Pepe I, Johansson B (2002) J Appl Phys 92:7219
9. Schieber M, Hermon H, Zuck A, Vilensky A, Melekhov L, Shatunovsky R, Meerson E, Saado Y, Lukach M, Pinkhasy E, Ready SE, Street RA (2001) J Cryst Growth 225:118
10. Dmitriev Y, Bennett PR, Cirignano LJ, Klugerman M, Shah KS (2008) Nucl Instrum Method A 584:165
11. Schieber M, Zamoshchik N, Khakhan O, Zuck A (2008) J Cryst Growth 310:3168
12. Fornaro L, Saucedo E, Mussio L, Gancharov A (2002) IEEE Trans Nucl Sci 49:2274
13. Ponpon JP, Amann M (2001) Thin Solid Films 394:277
14. Condeles JF, Martins TM, Dos Santos TC, Brunello CA, Rosolen JM, Mulato M (2004) J Non-Cryst Solids 338–340:81
15. McGregor DS, Hermon H (1997) Nucl Instrum Methods A 395:101
16. Hayashi T, Kinpara M, Wang JF, Mimura K, Isshiki M (2008) Cryst Res Technol 43(1):9
17. He Y, Zhu S, Zhao B, Jin Y, He Z, Chen B (2007) J Cryst Growth 300:448
18. Condeles JF, Ando RA, Mulato M (2008) J Mater Sci 43:525. doi:10.1007/s10853-007-1854-9
19. Unagami TJ (1999) Electrochem Soc 146:3110
20. Perednis D, Gauckler LJ (2005) J Electroceram 14:103
21. Siefert W (1984) Thin Solid Films 120(4):267
22. Yu HF, Liao WH (1998) Int J Heat Mass Transf 41(8–9):993
23. Ul Islam AKMF, Islam R, Khan KA (2005) Renew Energy 30:2289
24. Fornaro L, Saucedo E, Mussio L, Yerman L, Ma X, Burger A (2001) Nucl Instrum Methods A 458:406
25. Li HY, Zhang H, Li ZS, Li DM, He DY (2005) J Inorg Mater 20(5):1239
26. Matuchova M, Zdansky K, Svatuska M, Zavadil J, Prochazkova O (2007) Chem Pap 61(1):36
27. Oliveira IB, Costa FE, Armelin MJ, Cardoso LP, Hamada MM (2002) IEEE Trans Nucl Sci 49(4):1968
28. Matuchova M, Zdansky K, Zavadil J, Maixner J, Alexiev D, Prochazkova D (2006) Mater Sci Semicond Process 9:394